THE JOURNAL OF PHYSICAL CHEMISTRY B

Article

pubs.acs.org/JPCB

Elastic Phases of $Ge_xSb_xSe_{100-2x}$ Ternary Glasses Driven by Topology

Kapila Gunasekera,[†] P. Boolchand,[†,*] and M. Micoulaut[‡]

[†]Department of Electrical and Computing Systems, College of Engineering and Applied Science, University of Cincinnati, Cincinnati, Ohio 45221-0030, United StatesUSA

[‡]Laboratoire de Physique Théorique de la Matière Condensée, Université Pierre et Marie Curie, Boite 121, 4, Place Jussieu, 75252 Paris Cedex 05, France

Supporting Information

ABSTRACT: Topology offers a practical set of computational tools to accurately predict certain physical and chemical properties of materials including transformations under deformation. In network glasses with increased cross-linking three generic elastic phases are observed. We examine ternary $Ge_xSb_xSe_{100-2x}$ glasses in Raman scattering, modulated DSC and volumetric measurements, and observe the rigidity transition, $x = x_c(1) = 14.9\%$ that separates the flexible phase from the Intermediate phase, and the stress transition, $x = x_c(2) = 17.5\%$ that separate the intermediate phase from the stressed rigid one. Raman scattering provides evidence of the structural motifs populated in these networks. Using size increasing cluster agglomeration, we have calculated the rigidity and stress transitions to occur near $x_c(1)^t = 15.2\%$ and $x_c(2)^t = 17.5\%$, respectively. Theory predicts and experiments confirm that these two transitions will coalesce if edge−sharing Ge-tetrahedral motifs were absent in the structure, a circumstance that prevails in the Ge-deficient $Ge_7Sb_xSe_{93-x}$ ternary, underscoring the central role played by topology in network glasses. We have constructed a global elastic phase diagram of the Ge−Sb−Se ternary that provides a roadmap to network functionality. In this diagram, regions labeled A, B, and C comprise networks that are flexible, rigid but unstressed, and stressed-rigid, respectively.

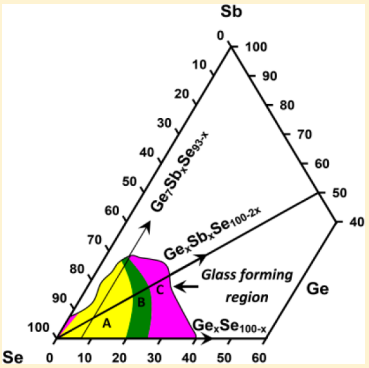

1. INTRODUCTION

In soft matter, applications of topology include foams,[1,2] quasicrystals,[3] nonuniform media,[4] and glasses.[5−7] Concerning the latter, a topological approach to rigidity theory has provided new insights[8] into understanding glassy covalent networks. It has led to the recognition of elastic phase transitions[9] separating flexible glassy networks having internal degrees of freedom that allow for local deformations, from stressed rigid ones which are "locked" by their high connectivity.

In a global approach to rigidity one has found it useful to analyze physical properties of multicomponent systems in terms of their network connectivity, measured in terms of mean coordination number "r".[9] Characteristic structural motifs composed of tetrahedra (edge and/or corner-sharing), pyramids, and quasi-tetrahedra play an important role in understanding network properties including their elastic phases. The use of the term phase within Rigidity theory[8,10] is to denote changes in physical properties of network glasses with composition. Recently, it was shown[11] that the increase of fragility in tetrahedral glass-forming liquids could be quantitatively understood from an increase in edge-sharing (ES) fraction of group IV (Si, Ge) tetrahedra in binary selenide glasses. Experiments[12] supported by theory[8,13] have also shown the existence of two elastic phase transitions in network glasses, a *rigidity* transition followed by a *stress* transition with increasing r. Glass compositions in between these transitions, the intermediate phase (IP), have evoked special interest both at a basic level and in applications because of their most unusual physical properties including absence of network stress,[14] nonaging,[15] and space filling property.[12]

In the above respect, the case of group V sulfides and selenides has received less attention than the group IV ones, even though IPs in the P−Se,[16,17] P−S,[18] and As−Se[19] and As−S[20] binaries are established. The case of the Sb_xSe_{100-x} binary would appear to be of marginal interest given that homogeneous glass formation is restricted[21] to $x < 2$ at % of Sb with the larger size and more metallic pnictide. However, experiments reveal[6] that by alloying a few mol % of Ge, glass formation can be extended over an increased range of Sb in the $Ge_7Sb_xSe_{93-x}$ ternary. More spectacular is the fact that in the $Ge_xSb_xSe_{100-2x}$ ternary, containing equimolar concentrations of Ge and Sb, glass formation extends over a much wider range ($0 < x < 22\%$) of Sb or a mean coordination number in the $2.00 < r < 2.62$ range.[22] We take Ge, Sb, and Se to be, respectively, 4-, 3- and 2- fold coordinated, yielding $r = 2 + 3x$. We have examined the $Ge_xSb_xSe_{100-2x}$ ternary in Raman scattering and modulated DSC experiments, and in this paper show that the rigidity and stress transitions appear respectively, near $r_c(1) = 2.42(1)$ and $r_c(2) = 2.52(1)$. Using size increasing cluster approximation[8] (SICA) and the four structural motifs observed in Raman studies, we attempt to predict these transitions. SICA in its simplest form, i.e., in the first level of approximation,

Received: May 8, 2013
Revised: June 28, 2013
Published: July 25, 2013

   dx.doi.org/10.1021/jp404565d | J. Phys. Chem. B 2013, 117, 10027−10034

already reproduces the salient features observed in experiments. These findings when compared to those reported earlier on corresponding P- and As- bearing ternaries[15,23] highlight the role of topology at a local level, coordination numbers of structural motifs, and on extended scale, fraction of ES/CS units, to determine these elastic phase transitions. Taken together, these results on $Ge_xPn_xSe_{100-2x}$ ternaries, with the Pn = P, As, and Sb, provide a unified view of elastic phase transitions observed in these ternary covalent selenides.

2. EXPERIMENTAL SECTION

Bulk ternary $Ge_xSb_xSe_{1-2x}$ alloy glasses over the range, $0 < x < 22\%$, were synthesized starting from 99.999% Ge, Sb and Se pieces (3 mm diam.) from Cerac Inc. The starting materials, sealed in evacuated (10^{-7}Torr) 5 mm ID quartz tubings, were alloyed at 950 °C for periods ranging from 5 to 10 days, and quenched from 50 °C above the liquidus in cold water to realize bulk samples. FT-Raman spectra, taken along the length of a quartz tube encapsulating a melt-quenched glass, were taken over the 5−10 day alloying period, until all line-shapes coalesced into a single one (see Figure S1of the Supporting Information, SI), at which point sample compositions were considered homogeneous. This novel technique was recently introduced[7,24−26] to ascertain batch homogeneity, and has been remarkably powerful in synthesis of homogeneous chalcogenides melts/glasses. Mass density of the glasses was established using Archimedes' principle. A quartz fiber attached to a digital balance was used to weigh samples in air and in pure ethyl alcohol. A single crystal of Si was used to calibrate the density of alcohol, and a single crystal of Ge used to check accuracy of measurements. Modulated DSC experiments used a model 2920 instrument from TA Instruments, and scans were taken at 3 °C/min ramp rate with a sinusoidal modulation of 1 °C temperature modulation, and 100 s modulation time. After scanning up in temperature to T_g + 25 °C, a cool-down cycle was programmed, and the frequency correction to the nonreversing enthalpy made in the usual way.[27−29] Compositional trends in $T_g(x)$, and nonreversing enthalpy, $\Delta H_{nr}(x)$, were measured on T_g-cycled samples both in the fresh (rejuvenated) and aged state. Aging was performed at room temperature $T < T_g$ with samples sealed in hermetically sealed Al pans. Figure 1 provides a summary of compositional trends in $T_g(x)$, $\Delta H_{nr}(x)$, and molar volumes $V_m(x)$. We note that $T_g(x)$ increases monotonically in the $0 < x < 18.2\%$ range, but decreases thereafter, which is signature of demixing[30] of homopolar bonds (Ge−Ge, Sb−Sb) formed above the chemical threshold (Figure 1, inset). The $\Delta H_{nr}(x)$ term shows a deep and sharp reversibility window in the $14.2\% < x < 17.5\%$ range, and the term is found to age outside the window but not in it over months. In the same composition range, molar volumes show a local minimum. T_g's and molar volumes of the present samples are found to be measurably higher than earlier reports[22,31] (Figure 1), probably because of their dryness and homogeneity.

FT-Raman scattering measurements made use of Thermo-Nicolet Model Nexus 870 unit with a laser spot size of 250 μm to profile melts. Raman spectra at select compositions are shown in Figure 2 . Observed lineshapes were deconvoluted to superposition of appropriate number of Gaussians to extract variations in mode scattering strength and frequency with x. In the Se-rich regime ($x < 18.2\%$), we observe several modes, which were noted earlier in binary Ge_xSe_{100-x} glasses[7,24,25] that result from Ge centered cross-linking structures (see below)

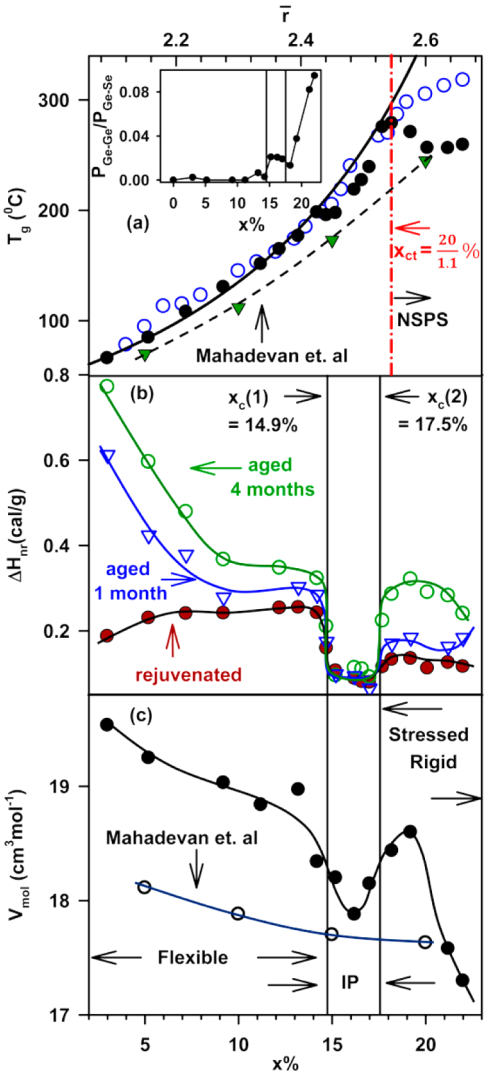

Figure 1. Filled circle data points show trends in (a) $T_g(x)$, (b) $\Delta H_{nr}(x)$, and (c) $V_m(x)$ in the present $Ge_xSb_xSe_{100-2x}$ ternary. In (a) we compare the present results (●) with those on the $Ge_xSb_xSe_{100-2x}$ ternary by Mahadevan et al (▼)[22] and the $Ge_xAs_xSe_{100-2x}$ ternary (○) by T. Qu et al.[23] The inset in (a) shows the fraction of Ge−Ge/Ge−Se bonds derived from a stochastic agglomeration theory (SAT) based analysis of $T_g(x)$ variation.[32] Note that $T_g(x)$ in the present ternary shows a kink near x = 18.2%, which identifies the chemical threshold. Such a kink is not observed in $Ge_xAs_xSe_{100-2x}$ glasses. The smooth line is a prediction of $T_g(x)$ based on SAT for the present ternary. In (b) we show the presence of aging of the $\Delta H_{nr}(x)$ term outside the reversibility window but not in it. In (c) we compare the present molar volumes to those reported by Mahadevan et al.[22]

formed with polymeric Se-chains. In addition, we observe other modes that are due to pyramidal $SbSe_3$ units. In the Se-deficient regime ($x > 18.2$ at %), new modes appear (see the SI) that can be assigned to homopolar bonds, Ge−Ge and Sb−Sb, the former as part of ethanelike units (Ge_2Se_3) and the latter as part of ethylenelike units ($Sb_2Se_2(Se_{1/2})_4$. We are guided in Raman mode assignments by first principles cluster calculations[33,34] and by observed variations in mode scattering strengths with x (see the SI).

The systematic blue-shift of CS mode frequency (ν) with increasing x in the Se-rich regime confirms the blue-shift to be the result of increased network connectivity. From these data,

dx.doi.org/10.1021/jp404565d | J. Phys. Chem. B 2013, 117, 10027−10034

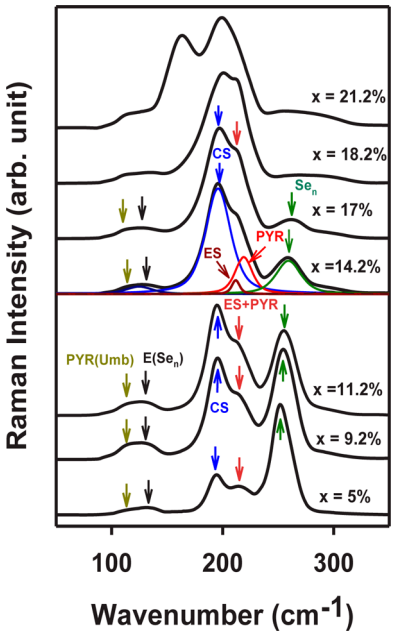

Figure 2. Observed Raman spectra of glass samples at indicated compositions in $Ge_xSb_xSe_{100-2x}$ ternary. Raman line shape at x = 14.2%, is deconvoluted into five Gaussian components, and these are identified with modes of CS $GeSe_4$ tetrahedra (195 cm^{-1}), ES tetrahedral (219 cm^{-1}), Pyramidal $Sb(Se_{1/2})_3$ units (215 cm^{-1}), Se_n-chain mode (260 cm^{-1}), PYR umbrella mode of $Sb(Se_{1/2})_3$ (115 cm^{-1}), and an E mode of Se_n chains (135 cm^{-1}) New modes identified with Sb−Sb and Ge−Ge bonds are observed in the Se-deficient phase (x > 18.2%), and are commented upon in the SI.

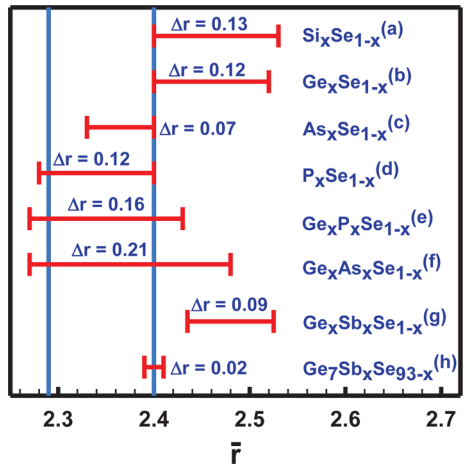

Figure 3. Intermediate phases observed in titled binary and ternary Selenides. The vertical lines drawn at r = 2.28 and 2.40 are for reference. Results on the titled glass systems are taken from (a) Selvanathan et al.,[42] (b) Bhosle et al.,[7] (c) Georgiev et al.,[43] (d) Georgiev et al.,[16] (e) S. Chakravarty et al.,[15] (f) T. Qu et al.,[23] (g) present work, and (h) Madhu et al.[6]

we deduce an elastic power-law of p = 1.20(5) in the IP for the corner-sharing mode frequency (ν) increase with x using,

$$\nu^2 - \nu_c^2 = A(x - x_c)^p \quad (1)$$

Here ν_c represents the mode frequency at the rigidity threshold x_c, and find the optical elastic power-law, p, to be in reasonable accord with earlier results.[15,23]

3. DISCUSSION

3.1. Topology and Elastic Phases. The observation of the sharply defined reversibility window (Figure 1b), permits fixing the *rigidity* and *stress* transitions near $x_c(1)$ = 14.9% and $x_c(2)$ = 17.5%, from the walls of the window. The feature of a vanishing nonreversing enthalpy at T_g in the IP phase has been noted earlier in many experiments,[12] and recently modeled in theory.[28] Thus, one views Se-rich glasses at x < 14.9% to be in the flexible phase, and Se-deficient ones at x > 17.5% to be in the stressed-rigid phase, while those in the intervening region to be in the IP. The local minimum of molar volumes (Figure 1c) in the IP is consistent with the compacted or space filling nature[35] of networks formed in this phase.

A salient feature of the present results on the $Ge_xSb_xSe_{100-2x}$ ternary is the onset of rigidity near $r_c(1)$ = 2.45, significantly upshifted in r (Figure 3) in relation to the cases of $Ge_xP_xSe_{100-2x}$ ($r_c(1)$ = 2.28) and $Ge_xAs_xSe_{100-2x}$ ($r_c(1)$ = 2.28) ternaries. There is strong evidence that P[15] and As[23] cations occur in pyramidal (PYR) (r = 2.40) as well as in quasi-tetrahedral (QT) structural motifs (r = 2.28) in respective ternary selenides, but Sb takes only the PYR configuration in the present ternary as no specific Raman signature for the QT species has been found for the present investigated system. The onset of the rigidity transition in the P- and As-based ternaries at lower r in relation to the Sb-based ternary is traced to the presence of QT motifs[23,36] that possess a low mean coordination number of r = 2.28. Onset of rigidity in these ternary glasses is determined by ring-like configurations[8] of the most Se-rich isostatic structural motifs formed. Network stress is a nonlocal property and much of the challenge to understanding IPs comes from the multiply connected nature of structure determined by network topology. The IP library (Figure 3), along with the structural motifs present in the backbone provides important bounds on realistic topological structural models of these phases. The excitement and challenge of IPs is that such networks adapt,[37] reconnect to lower their free energy, i.e., self-organize during melt quench.

The stressed-rigid phase forms at x > 17.5%, and glassy networks in this phase are largely demixed (see below), a feature also found[38] in the 225 phase change material ($Ge_2Sb_2Te_5$ or x = 22.2%) in corresponding $Ge_xSb_xTe_{100-2x}$ Tellurides as well as other systems.[32] The nature of chemical bonding in the present ternary, as suggested by the observed elastic phases is covalent as atoms conform to the 8-N bonding rule. This is an important result in its own right given that in corresponding amorphous-Tellurides, the bonding rule is intrinsically broken[39] as Pauling resonant bonding effects prevail as found in their crystalline counterparts.[40] Knowledge of the elastic phases in the $Ge_xSb_xTe_{100-2x}$ ternary tellurides[40] will undoubtedly help better understand their functionality as phase-change materials.

3.2. Glass Structure and Onset of a Chemical Threshold. Our Raman scattering results suggest that Se-rich glasses (x < 18.2%) largely consist of polymeric Se_n chains that are progressively cross-linked by 4-fold Ge and 3-fold Sb, thus locally satisfying their chemical bonding valence requirements. The local structures formed at the cross-links consist of CS- and ES- $GeSe_4$ tetrahedra and pyramidal $SbSe_3$. Stoichiometrically, one can write,

$$Ge_xSb_xSe_{100-2x} = Ge_xSe_{2x} + Sb_xSe_{3/2x} + Se_{100-2x-2x-3/2x} \quad (2)$$

dx.doi.org/10.1021/jp404565d | J. Phys. Chem. B 2013, 117, 10027−10034

Table 1. SICA Structures with Their General Probabilities (Not Normalized), Their Estimate in Case of Self-Organization, And the Associated Number of Constraints n_c

Cluster Structures	Probability (not normalized)	Probabilities (not normalized) using equs. (6a,6b) in the self-organized case	n_c
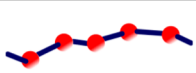	$4P_S{}^2e_{flex}$	$\frac{8(2-11x)(72xe_{ring}+4-31x)}{3(2-3x)^2}$ if $x<x_c$; 0 if $x>x_c$	2.0
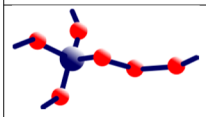	$16P_SP_Ge_{iso}$	$\frac{64(2-11x)x}{(2-3x)^2}$	3.0
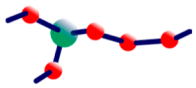	$12P_SP_{Sb}e_{flex}$	$\frac{32x(72xe_{ring}+4-31x)}{(2-3x)^2}$ if $x<x_c$; 0 if $x>x_c$	2.56
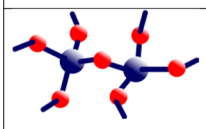	$16P_G{}^2e_{stress}$	0 if $x<x_c$; $\frac{16x(31x-4-72xe_{ring})}{(2-3x)^2}$ if $x>x_c$	3.67
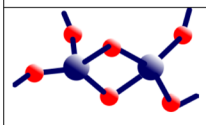	$72P_G{}^2e_{ring}$	$\frac{1152x^2e_{ring}}{(2-3x)^2}$	3.25
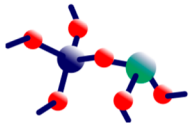	$24P_GP_{Sb}e_{stress}$	0 if $x<x_c$; $\frac{24x(31x-4-72xe_{ring})}{(2-3x)^2}$ if $x>x_c$	3.36
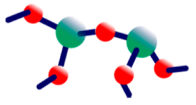	$9P_{Sb}{}^2e_{iso}$	$\frac{144x^2}{(2-3x)^2}$	3.0

with the last term on the right-hand side of eq 2 representing Se atoms left over in a polymeric chain configuration. The chemical threshold (ct) would then occur when the last term vanishes, i.e., $11x_{ct}/2 = 100$, or $x_{ct} = 18.2\%$. As $x > x_{ct}$, homopolar (Ge−Ge, Sb−Sb) bonds can be expected to appear in the network. Thus, glass compositions at $x < 18.2\%$ are viewed as Se-rich, while those at $x > 18.2\%$ as Se-deficient. In the Se-deficient glasses, a pertinent issue is- do the heteropolar bonds form part of the network backbone or do they segregate as Ge-rich and Sb-rich clusters? The $T_g(x)$ variation (Figure 1a filled circles) in the present ternary reveals a kink near $x = x_{ct}$, an observation that constitutes signature of homopolar bonds demixing from the backbone.[30] If these homopolar bonds were formed as part of the backbone, then one would expect $T_g(x)$ to monotonically increase past x_{ct} as predicted by Stochastic Agglomeration Theory[41] (Figure 1a smooth line), and as observed in the $Ge_xAs_xSe_{100-x}$ ternary.[30] Note that the covalent radii of Ge, As and Se are nearly the same in the $Ge_xAs_xSe_{100-x}$ ternary. The demixing of the $Ge_xSb_xSe_{100-2x}$ ternary at $x > x_{ct}$ is thought to be driven by atomic size mismatch (covalent radii, r_{cov} (Sb) = 1.40 Å, r_{cov} (As)= 1.20 Å, r_{cov} (Ge) = 1.22 Å, and r_{cov} (Se) = 1.17 Å).

In Raman scattering existence of Sb−Sb and Ge−Ge bonds is observed in Se-deficient glass compositions ($x > x_{ct}$). The growth in Raman activity in the 160−190 cm^{-1} range, starts already at $x = 18.2\%$ (compare spectrum at $x = 17.0\%$ with the one at $x = 18.2\%$ in Figure 2). Furthermore, there is growth in scattering in the high frequency (240 cm^{-1} to 330 cm^{-1}) range as can be seen by comparing the spectrum of a glass at $x = 22\%$ with the one at $x = 18.2\%$ (Figure 2). We identify these systematic changes in the observed lineshapes with composition as resulting from growth of Ge−Ge bonds present in an ethanelike cluster and Sb−Sb bonds in an ethylenelike cluster in these glasses. There are three characteristic vibrational modes (187 cm^{-1}, 216 cm^{-1}, and 234 cm^{-1}) of ethylenelike clusters and two (179 cm^{-1} and 288 cm^{-1}) of ethanelike clusters that are predicted.[33,34] from first principles calculations, and also observed in the spectra. We discuss these findings including Raman spectral deconvolution results in the SI. Another feature of the Raman results is that vibrational mode frequency of these clusters steadily red-shift as mode scattering strength increases at $x > x_{ct}$. The behavior apparently stems from cluster geometries changing as they grow in size and decouple from the backbone.

3.3. Size Increasing Cluster Approximation. SICA combined with rigidity theory permits predicting the elastic threshold for the rigidity and stress transition.[8,44] We build on the successful modeling of Group IV selenides and derive in a similar fashion clusters for the present ternary glass $Ge_xSb_xSe_{100-2x}$ which can be rewritten as (Ge-

dx.doi.org/10.1021/jp404565d | J. Phys. Chem. B 2013, 117, 10027−10034

$Se_{4/2})_x(SbSe_{3/2})_xSe_{100-11x/2}$. In these calculations, one agglomerates the basic structural motifs observed ($GeSe_{4/2}$ tetrahedra, $SbSe_{3/2}$ pyramids, and Se_2-chains) whose probabilities are given by stoichiometry, i.e.:

$$P_{Se_2} = \frac{2 - 11x}{2 - 3x} = 1 - P_G - P_{Sb} = P_S \quad (3a)$$

$$P_{GeSe_{4/2}} = P_{SbSe_{3/2}} = \frac{4x}{2 - 3x} = P_G = P_{Sb} \quad (3b)$$

for compositions $x < x_{ct}$, i.e., compositions for which homopolar Sb−Sb or Ge−Ge can be safely neglected.

From these initial probabilities P_i, one computes the probability of finding larger clusters.

We obtain a series of 7 different clusters (including ES $GeSe_{4/2}$ connections) represented in Table 1 with their corresponding probabilities and constraint count (see below). The probabilities of such clusters are given by the following:

$$P_{ij} = \frac{W_{ij}}{Z} P_i P_j e^{-E_{ij}/k_B T} \quad (4)$$

where the normalizing factor Z ensures that $\Sigma_{ij}\ P_{ij} = 1$. The term W_{ij} is a statistical factor which depends on the number of equivalent ways to connecting the starting species to yield a given cluster. For simplicity, we reduce the number of energy gains E_{ij} to three, depending on the elastic nature (flexible, intermediate, stressed rigid) of the considered cluster: E_{flex}, E_{iso}, E_{stress}. An additional energy, E_{ring}, is introduced for ring closure leading to ES connections. Due to the normalizing factor Z, the whole construction depends only on three parameters $e_i = \exp[(E_{iso} - E_i)/k_B T]$ with i = (flex, stress, ring). Two of these parameters can be exactly determined by writing a conservation equation for the species, i.e.,

$$P_{GG} + \frac{1}{2}P_{GS} + \frac{1}{2}P_{GSb} = x = P_{SbSb} + \frac{1}{2}P_{SbS} + \frac{1}{2}P_{GSb} \quad (5)$$

which can be solved in the chalcogen-rich ($e_{stress} = 0$) and chalcogen-poor ($e_{flex} = 0$) region of the phase diagram, leading respectively to the following:

$$e_{flex} = \frac{2(72xe_{ring} + 4 - 31x)}{3(2 - 11x)} \quad (6a)$$

$$e_{stress} = -\frac{(72xe_{ring} + 4 - 31x)}{16x} \quad (6b)$$

One also remarks that to be valid $e_i > 0$ (i = stress, flex), and thus one has a constraint on the compositional domain bounded by the concentration:

$$x_c = \frac{4}{31 - 72e_{ring}} \quad (7)$$

The composition x_c also represents $x_c(2)^t$ as discussed below. Equations 6a and 6b allow us to have the probabilities depend only on a single parameter e_{ring} (Table 1).

Note that the condition $e_i = 1$ (i = flex, ring, stressed) leads to the usual random bond distribution with probabilities only given by their statistical weight. In the latter case, CS or ES $GeSe_{4/2}$ connections have non-normalized probabilities, which are given by $16P_G^2$ and $72P_G^2$, respectively. Among this population of generated clusters, one can compute the probability of finding flexible ($n_c < 3$), isostatically rigid ($n_c = 3$) and stressed-rigid ($n_c > 3$) clusters. Here n_c represents the count of bonding constraints due to bond-stretching and bond-bending forces per atom. Various situations[8,44] can then be investigated: random bonding case, and self-organized case which amounts to avoid forming stressed- rigid CS connections as far as possible as x is steadily increased. This amounts requesting $e_{stress} = 0$ (eq 6b) as long as possible.

One identifies the *rigidity* transition by requiring the vanishing of the count of floppy modes ($f = 3 - n_c = 0$), and the stress transition x_c given by equ. 7 when CS stressed-rigid links can no longer be avoided as x increases. In the case of random connections, theory predicts a *single* transition near $r = 2.40$ or $x = 13.3\%$ (broken blue curve, Figure 4). This also

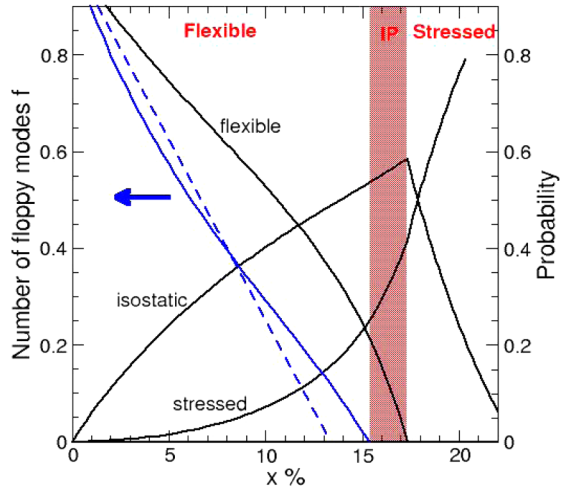

Figure 4. SICA results for $Ge_xSb_xSe_{100-x}$ glasses. Calculation of the number of floppy modes $f = 3 - n_c$ from the local structures (broken blue line) and from self-organized clusters having a finite fraction of ES motifs (solid blue line). The latter defines the Rigidity Transition (RT) at 15.3%. Right axis: probability (black solid lines) of finding flexible, isostatic (which peaks at the Stress Transition near 17.2%) and stressed rigid clusters as function of composition. The pink zone defines the IP.

corresponds to the result obtained from a direct constraint count on the initial local structures ($GeSe_{4/2}$ tetrahedra, $SbSe_{3/2}$ pyramids and Se_2-chains). In the case of self-organized networks (avoidance of CS connections as long as possible, see Table 1), and with a finite fraction of ES motifs as the only adjustable parameter in the theory, calculations predict (i) the rigidity transition (RT) to upshift in x or r (solid blue curve, Figure 4), and (ii) the RT and the stress-transition (ST) to split, and to occur near $x_c(1)^t = 15.3\%$ and near $x_c(2)^t = 17.2\%$ (right axis, Figure 4) for, e.g., at an ES/CS fraction η of 1.4 at a fixed composition of $x = 18.18\%$. In fact, e_{ring} can be expressed as a function of the ES to CS ratio defined by the following:

$$\eta = \frac{P^{ES}_{GG}}{P^{CS}_{GG}} = \frac{9e_{ring}}{e_{stress}} \quad (8)$$

and using eq 6b, one has the following:

$$e_{ring} = \frac{13\eta}{72(\eta + 1)} \quad (9)$$

at $x = x_{ct} = 18.18\%$.

Our SICA predictions are is excellent accord (Figure 5) with the experimental results if the ES/CS fraction is taken to be about 1−1.7, of the same order to what is obtained (1.17) from

dx.doi.org/10.1021/jp404565d | J. Phys. Chem. B 2013, 117, 10027−10034

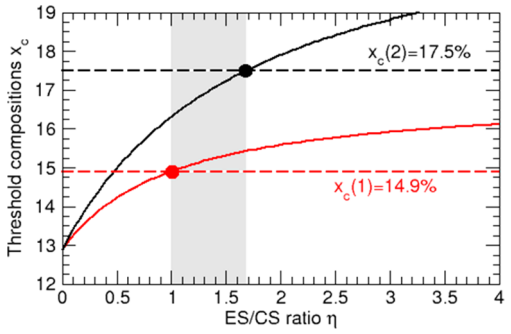

Figure 5. SICA results for the location of the rigidity (red curve) and stress transition (black curve) as a function of the ES/CS ratio. The broken horizontal lines correspond to the experimentally determined transitions $x_c(1)$ and $x_c(2)$ and the intercept with the SICA result provides an estimation of η (between 1 and 1.7, gray zone).

Molecular Dynamics simulations[45] for a similar system ($GeSe_2$). The experimental results of the ES/CS ratio come from Raman scattering and requires knowledge of the scattering cross-section of the ES and CS vibrational modes to convert the observed scattering strength ratio of about 1/2 to reliably determine ES/CS fraction. At present, there are no reliable estimates of these matrix elements effects to deduce the ES/CS fraction. It is also possible that if the agglomeration steps in SICA are extended to higher level, a smaller ES/CS fraction would suffice to understanding the observed thresholds of the rigidity- and stress-transitions in the present $Ge_xSb_xSe_{100-2x}$ ternary. We plan to explore these possibilities in future studies.

3.4. Global Elastic Phase Diagram of the Ge–Sb–Se ternary. Given the present results on the $Ge_xSb_xSe_{100-2x}$ ternary, and those on the Ge_tSe_{100-t} binary,[24,25] it is possible to construct a global elastic phase diagram of the present Ge–Sb–Se ternary as shown in Figure 6. It is useful to recall that in the Sb_ySe_{100-y} binary, homogeneous glass formation is restricted to a rather small concentration, $y < 0.02$ of Sb as noted earlier.[21,46] At higher concentrations, Sb tends to cluster as a nanocrystalline Sb_2Se_3 moiety in Se–rich glasses, as suggested by the glass transition temperature remaining essentially close to 40 °C, the value characteristic of Se-glass, while displaying a slope $dT_g/dy = T_g(y = 0)/\ln(3/2)$ for $y < 1\%$ in agreement with SAT predictions.[21] The glass forming tendency of binary Ge_xSe_{100-x} glasses and their elastic phases have been extensively studied over the years, and the recent results[24,25] on homogeneous glasses are included in Figure 6.

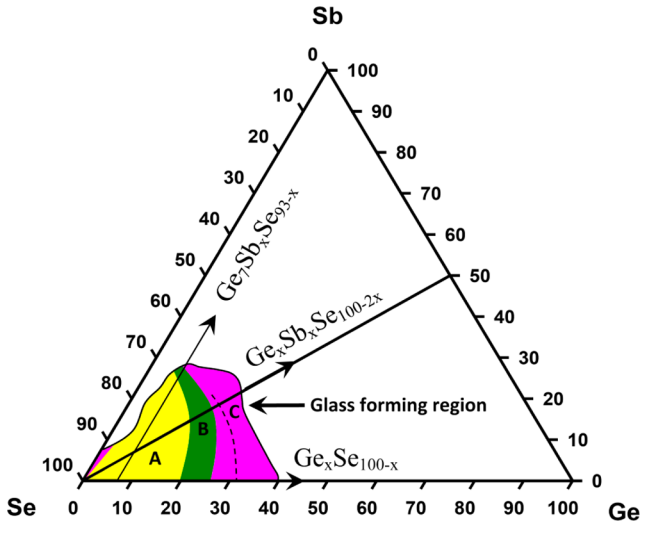

Figure 6. Global elastic phase diagram of bulk Ge–Sb–Se ternary glasses constructed from the established elastic phases in the Ge_xSe_{100-x} binary,[7] $Ge_7Sb_xSe_{93-x}$ ternary,[6] and the present work on $Ge_xSb_xSe_{100-2x}$ ternary. Phases are indicated as flexible (A, yellow), intermediate (B, green), and stressed rigid (C, indigo). The chemical threshold phase boundary is shown by the black dashed line and resides in the Stressed-rigid phase. The glass forming region is taken from Sreeram et al.[31] and Borisova et al.[47]

Madhu et al. reported[6] observing a narrow ($\Delta r = 0.02$) IP centered near $x = 26\%$ or $r = 2.40$ in the Ge-deficient $Ge_7Sb_xSe_{93-x}$ ternary (Figure 3). In this ternary, as in the case of the base Ge_7Se_{93} binary, Raman scattering unambiguously shows absence of ES $GeSe_2$ tetrahedral units. These structural motifs are first manifested when the Ge concentration x exceeds about 12% in binary Ge_xSe_{100-x} glasses. Thus, theory and experiment come together in revealing that the narrowing of the IP width in the $Ge_7Sb_xSe_{93-x}$ ternary stems from absence of ES motifs.

From the above cited reports one can now construct a global elastic phase diagram of the present Ge–Sb–Se ternary (Figure 6). Se-rich bulk glasses composed of Se_n chains are elastically floppy[48] and comprise the Flexible phase of the present ternary shown as the A (yellow)-region in Figure 6. Upon progressive cross-linking by alloying both Ge and Sb, a rigid but unstressed elastic phase, Intermediate phase, manifests in the B (green)-region. This phase is of special interest in applications because of its unstressed nature by virtue of topology. And as one cross-links the network further by alloying more Sb and Ge, the stressed-rigid elastic phase C(indigo) is manifested. Stressed-rigid glassy networks eventually demix,[32] a feature observed in the present glasses as well. A parallel elastic phase diagram in corresponding ternary sulfides, Ge–Sb–S, probably exists although studies[49] to date have not been directed toward that goal.[31,47]

4. CONCLUSIONS

In summary, topology and connectivity determined by local structural motifs (Figure 4) provides a useful basis to quantitatively understand the three elastic phases of ternary $Ge_xPn_xSe_{100-2x}$ glasses, with Pn = P, As, Sb. In these polymerized networks, the ring topology and connectivity of the most Se-rich isostatic local structural motif determines the Rigidity transition, while percolation of the most Se-deficient structural motif the Stress transition. Presence of a multitude of isostatic local structural motifs with variable stoichiometry can be used to design wide IPs in multicomponent network glasses for applications. In this work, we present the first example of a global phase diagram in Sb bearing chalcogenides established experimentally and supported by theory. Such materials are the active element of phase change memories.[50]

■ ASSOCIATED CONTENT

Supporting Information

Details on synthesis of bulk glasses, and particularly a check on their structural homogeneity by FT-Raman profiling experiments. Raman vibrational modes characteristic of homopolar Ge–Ge and Sb–Sb bonds. Results of numerical simulations of IR and Raman active modes of ethane-like (Ge_2Se_6) and ethylene-like (Sb_2Se_4) clusters containing homopolar bonds of interest. Predictions from first principles cluster calculations

dx.doi.org/10.1021/jp404565d | J. Phys. Chem. B 2013, 117, 10027–10034

compared to the observed modes. Observed Raman spectra of Se-deficient glasses at $x > 18.2\%$ are deconvoluted, and observed modes identified. Comparison of the predicted and observed mode frequencies and particularly the scattering strength variation of the observed modes with x providing for consistency of mode assignments. This material is available free of charge via the Internet at http://pubs.acs.org.

AUTHOR INFORMATION

Corresponding Author

*Phone: 513-556-4790; e-mail: boolchp@ucmail.uc.edu.

Notes

The authors declare no competing financial interest.

ACKNOWLEDGMENTS

It is our pleasure to thank Professor Darl McDaniel and Professor K.A. Jackson for discussions during the course of this work, and especially for the first principles cluster calculations that facilitated Raman mode assignments. The work at University of Cincinnati is supported by US NSF grant DMR 08-53957, and at University Pierre et Marie Curie, Paris, by Agence Nationale de la Recherche (ANR) n.09-BLAN-0190-01, France.

REFERENCES

(1) Delaney, G. W.; Weaire, D.; Hutzler, S. Onset of Rigidity for Stretched String Networks. *Europhys. Lett.* **2005**, *72*, 990−996.

(2) Cerisier, P.; Rahal, S.; Rivier, N. Topological Correlations in Benard-Marangoni Convective Structures. *Phys. Rev. E* **1996**, *54*, 5086−5094.

(3) Dina Maria dos, S.-L.; Richard, K. Dynamique de la Croissance de Réseaux bi-Dimensionnels. *J. Phys. I France* **1994**, *4*, 1491−1511.

(4) Trub, A.; Trebin, H. R. Topology of the Phason Degree-of-Freedom, Phason Singularities, and Diffusive Motion in Octogonal Quasi-crystals. *J. Physiq. I* **1994**, *4*, 1855−1866.

(5) Salmon, P. S.; Barnes, A. C.; Martin, R. A.; Cuello, G. J. Glass Fragility and Atomic Ordering on the Intermediate and Extended Range. *Phys. Rev. Lett.* **2006**, *96*, 235502−235504.

(6) Madhu, B. J.; Jayanna, H. S.; Asokan, S. Evidence of an Intermediate Phase in Ternary $Ge_7Se_{93-x}Sb_x$ Glasses. *Eur. Phys. J. B—Condens. Matter Complex Syst.* **2009**, *71*, 21−25.

(7) Bhosle, S.; Gunasekera, K.; Chen, P.; Boolchand, P.; Micoulaut, M.; Massabrio, C. Meeting Experimental Challenges to Physics of Network Glasses: Assessing the Role of Sample Homogeneity. *Solid State Commun.* **2011**, *151*, 1851−1855.

(8) Micoulaut, M.; Phillips, J. C. Rings and Rigidity Transitions in Network Glasses. *Phys. Rev. B* **2003**, *67*, 104204−104209.

(9) Thorpe, M. F.; Jacobs, D. J.; Chubynsky, M. V.; Phillips, J. C. Self-Organization in Network Glasses. *J. Non-Cryst. Solids* **2000**, *266*, 859−866.

(10) Mauro, J. C. Topological Constraint Theory of Glass. *Am. Ceram. Soc. Bull.* **2011**, *90*, 31−37.

(11) Wilson, M.; Salmon, P. S. Network Topology and the Fragility of Tetrahedral Glass-Forming Liquids. *Phys. Rev. Lett.* **2009**, *103*, 157801−157804.

(12) Micoulaut, M.; Popescu, M. *Rigidity and Boolchand Intermediate Phases in Nanomaterials*: INOE: Bucharest, 2009, Vol. *6*.

(13) Chubynsky, M. V.; Briere, M. A.; Mousseau, N. Self-Organization with Equilibration: A Model for the Intermediate Phase in Rigidity Percolation. *Phys. Rev. E* **2006**, *74*, 016116−016119.

(14) Wang, F.; Mamedov, S.; Boolchand, P.; Goodman, B.; Chandrasekhar, M. Pressure Raman Effects and Internal Stress in Network Glasses. *Phys. Rev. B* **2005**, *71*, 174201−174208.

(15) Chakravarty, S.; Georgiev, D. G.; Boolchand, P.; Micoulaut, M. Ageing, Fragility and the Reversibility Window in Bulk Alloy Glasses. *J. Phys.: Condens. Matter* **2005**, *17*, L1−L7.

(16) Georgiev, D. G.; Boolchand, P.; Eckert, H.; Micoulaut, M.; Jackson, K. The Self-Organized Phase of Bulk P_xSe_{1-x} Glasses. *Europhys. Lett.* **2003**, *62*, 49−55.

(17) Lathrop, D.; Eckert, H. Chemical Disorder in Non-oxide Chalcogenide Glasses. Site Speciation in the System Phosphorus-Selenium by Magic Angle Spinning NMR at Very High Spinning Speeds. *J. Phys. Chem.* **1989**, *93*, 7895−7902.

(18) Boolchand, P.; Chen, P.; Vempati, U. Intermediate Phases, Structural Variance and Network Demixing in Chalcogenides: The Unusual Case of Group V Sulfides. *J. Non-Cryst. Solids* **2009**, *355*, 1773−1785.

(19) Chen, P.; Boolchand, P.; Georgeiv, D. Long Term Aging of Selenide Glasses: Evidence of Sub-T_g Endotherms and Pre-T_g exotherms. *J. Phys.: Condens. Matter* **2010**, *22*, 065104.

(20) Chen, P.; Holbrook, C.; Boolchand, P.; Georgiev, D. G.; Jackson, K. A.; Micoulaut, M. Intermediate Phase, Network Demixing, Boson and Floppy Modes, and Compositional Trends in Glass Transition Temperatures of Binary As_xS_{1-x} system. *Phys. Rev. B* **2008**, *78*, 224208.

(21) Tonchev, D.; Kasap, S. O. Thermal Properties of Sb_xSe_{100-x} Glasses Studied by Modulated Temperature Differential Scanning Calorimetry. *J. Non-Cryst. Solids* **1999**, *248*, 28−36.

(22) Mahadevan, S.; Giridhar, A.; Singh, A. K. Elastic Properties of Ge−Sb−Se Glasses. *J. Non-Cryst. Solids* **1983**, *57*, 423−430.

(23) Qu, T.; Georgiev, D. G.; Boolchand, P.; Micoulaut, M. In *Supercooled Liquids, Glass Transition and Bulk Metallic Glasses*; Egami, T., Ed.; Materials Research Society: Warrendale, PA, 2003; p 157.

(24) Bhosle, S.; Gunasekera, K.; Boolchand, P. Melt Homogenization and Self Organization in Chalcogenide Glasses—Part 2. *Intl. J. App. Glass. Sci.* **2012**, *3*, 205−220.

(25) Bhosle, S.; Gunasekera, K.; Boolchand, P.; Micoulaut, M. Melt Homogenization and Self Homogenization in Chalcogenides—Part 1. *Intl. J. App. Glass. Sci.* **2012**, *3*, 189−204.

(26) Boolchand, P.; Gunasekera, K.; Bhosle, S. Midgap States, Raman Scattering, Glass Homogeneity, Percolative Rigidity and Stress Transitions in Chalcogenides. *Phys. Stat. Solidi B* **2012**, 1−6.

(27) Thomas, L. C. *Modulated DSC Technology (MSDC-2006)*; T.A. Instruments, Inc (www.tainstruments.com): New Castle, DE, 2006.

(28) Micoulaut, M. Linking Rigidity With Enthalpic Changes at the Glass Transition and the Fragility of Glass-Forming Liquids: Insight from a Simple Oscillator Model. *J. Phys.: Condens. Matter* **2010**, *22*, 1−7.

(29) Guo, X.; Mauro, J. C.; Allan, D. C.; Yue, Y. On the Frequency Correction in Temperature-Modulated Differential Scanning Calorimetry of the Glass Transition. *J. Non-Cryst. Solids* **2012**, *358*, 1710−1715.

(30) Boolchand, P.; Georgiev, D. G.; Qu, T.; Wang, F.; Cai, L. C.; Chakravarty, S. Nanoscale Phase Separation Effects near $< r \geq 2.4$ and 2.67, and Rigidity Transitions in Chalcogenide Glasses. *Compt. Rend. Chim.* **2002**, *5*, 713−724.

(31) Sreeram, A. N.; Varshneya, A. K.; Swiler, D. R. Molar Volume and Elastic Properties of Multicomponent Chalcogenide Glasses. *J. Non-Cryst. Solids* **1991**, *128*, 294−309.

(32) Mamedov, S.; Georgiev, D. G.; Qu, T.; Boolchand, P. Evidence for Nanoscale Phase Separation of Stressed-Rigid Glasses. *J. Phys.: Condens. Matter* **2003**, *15*, S2397−S2411.

(33) Jackson, K.; Briley, A.; Grossman, S.; Porezag, D. V.; Pederson, M. R. Raman-Active Modes of a-$GeSe_2$ and a-GeS_2: A First-Principles Study. *Phys. Rev. B* **1999**, *60*, R14985−R14989.

(34) Jackson personal communication.

(35) Bourgel, C.; Micoulaut, M.; Malki, M.; Simon, P. Molar Volume Minimum and Adaptative Rigid Networks in Relationship with the Intermediate Phase in Glasses. *Phys. Rev. B* **2009**, *79*, 024201.

(36) Wang, Y.; Boolchand, P.; Micoulaut, M. Glass Structure, Rigidity Transitions and the Intermediate Phase in the Ge-As-Se ternary. *Europhys. Lett.* **2000**, *52*, 633−639.

(37) Barre, J.; Bishop, A. R.; Lookman, T.; Saxena, A. Adaptability and "Intermediate Phase" in Randomly Connected Networks. *Phys. Rev. Lett.* **2005**, *94*, 208701−208704.

(38) Raoux, S.; Wuttig, M. *Phase Change Materials, Science and Applications*; Springer: New York, 2009, p 446.
(39) Micoulaut, M.; Otjacques, C.; Raty, J.-Y.; Bichara, C. Understanding Phase-Change Materials from the Viewpoint of Maxwell Rigidity. *Phys. Rev. B* **2010**, *81*, 1−11.
(40) Shportko, K.; Kremers, S.; Woda, M.; Lencer, D.; Robertson, J.; Wuttig, M. Resonant Bonding in Crystalline Phase-Change Materials. *Nat. Mater.* **2008**, *7*, 653−658.
(41) Micoulaut, M. The Slope Equations: A Universal Relationship Between Local Structure and Glass Transition Temperature. *Eur. Phys. J. B* **1998**, *1*, 277−294.
(42) Selvanathan, D.; Bresser, W. J.; Boolchand, P.; Goodman, B. Thermally Reversing Window and Stiffness Transitions in Chalcogenide Glasses. *Solid State Commun.* **1999**, *111*, 619−624.
(43) Georgiev, D. G.; Boolchand, P.; Micoulaut, M. Rigidity Transitions and Molecular Structure of As_xSe_{1-x} glasses. *Phys. Rev. B* **2000**, *62*, R9228−R9231.
(44) Micoulaut, M. Rigidity and Intermediate Phases in Glasses driven by Speciation. *Phys. Rev. B* **2006**, *74*, 184208−184205.
(45) Massobrio, C.; Micoulaut, M.; Salmon, P. S. Impact of the Exchange-Correlation Functional on the Structure of Glassy $GeSe_2$. *Solid State Sci.* **2010**, *12*, 199−203.
(46) Kostadinova, O.; Yannopoulos, S. N. Raman Spectroscopic Study of Sb_xSe_{100-x} Phase-Separated Bulk Glasses. *J. Non-Cryst. Solids* **2009**, *355*, 2040−2044.
(47) Borisova, Z. U., *Glassy Semiconductors*; Plenum Press: New York, 1981.
(48) Kamitakahara, W. A.; Cappelletti, R. L.; Boolchand, P.; Halfpap, B.; Gompf, F.; Neumann, D. A.; Mutka, H. Vibrational Densities of States and Network Rigidity in Chalcogenide Glasses. *Phys. Rev. B* **1991**, *44*, 94−100.
(49) Lin, C.; Li, Z.; Ying, L.; Xu, Y.; Zhang, P.; Dai, S.; Xu, T.; Nie, Q. Network Structure in GeS_2−Sb_2S_3 Chalcogenide Glasses: Raman Spectroscopy and Phase Transformation Study. *J. Phys. Chem. C* **2012**, *116*, 5862−5867.
(50) Boolchand, P.; Micoulaut, M.; Chen, P. In *Phase Change Materials, Science and Applications*; Raoux, S., Wuttig, M., Eds; Springer: Heidelberg, 2009; pp 37−60.